Measurement of the total cross section for $e^+e^- \rightarrow$ hadrons at $\sqrt{s} = 10.52$ GeV

R. Ammar, P. Baringer, A. Bean, D. Besson, D. Coppage, C. Darling, R. Davis, N. Hancock, S. Kotov, I. Kravchenko, and N. Kwak
University of Kansas, Lawrence, Kansas 66045

S. Anderson, Y. Kubota, M. Lattery, S. J. Lee, J. J. O'Neill, S. Patton, R. Poling, T. Riehle, V. Savinov, and A. Smith
University of Minnesota, Minneapolis, Minnesota 55455

M. S. Alam, S. B. Athar, Z. Ling, A. H. Mahmood, H. Severini, S. Timm, and F. Wappler
State University of New York at Albany, Albany, New York 12222

A. Anastassov, S. Blinov,* J. E. Duboscq, K. D. Fisher, D. Fujino,† K. K. Gan, T. Hart, K. Honscheid, H. Kagan, R. Kass, J. Lee, M. B. Spencer, M. Sung, A. Undrus,* R. Wanke, A. Wolf, and M. M. Zoeller
Ohio State University, Columbus, Ohio 43210

B. Nemati, S. J. Richichi, W. R. Ross, P. Skubic, and M. Wood
University of Oklahoma, Norman, Oklahoma 73019

M. Bishai, J. Fast, E. Gerndt, J. W. Hinson, N. Menon, D. H. Miller, E. I. Shibata, I. P. J. Shipsey, and M. Yurko
Purdue University, West Lafayette, Indiana 47907

L. Gibbons, S. Glenn, S. D. Johnson, Y. Kwon, S. Roberts, and E. H. Thorndike
University of Rochester, Rochester, New York 14627

C. P. Jessop, K. Lingel, H. Marsiske, M. L. Perl, D. Ugolini, R. Wang, and X. Zhou
Stanford Linear Accelerator Center, Stanford University, Stanford, California 94309

T. E. Coan, V. Fadeyev, I. Korolkov, Y. Maravin, I. Narsky, V. Shelkov, J. Staeck, R. Stroynowski, I. Volobouev, and J. Ye
Southern Methodist University, Dallas, Texas 75275

M. Artuso, A. Efimov, F. Frasconi, M. Gao, M. Goldberg, D. He, S. Kopp, G. C. Moneti, R. Mountain, S. Schuh, T. Skwarnicki, S. Stone, G. Viehhauser, and X. Xing
Syracuse University, Syracuse, New York 13244

J. Bartelt, S. E. Csorna, V. Jain, and S. Marka
Vanderbilt University, Nashville, Tennessee 37235

R. Godang, K. Kinoshita, I. C. Lai, P. Pomianowski, and S. Schrenk
Virginia Polytechnic Institute and State University, Blacksburg, Virginia 24061

G. Bonvicini, D. Cinabro, R. Greene, L. P. Perera, and G. J. Zhou
Wayne State University, Detroit, Michigan 48202

B. Barish, M. Chadha, S. Chan, G. Eigen, J. S. Miller, C. O'Grady, M. Schmidtler, J. Urheim, A. J. Weinstein, and F. Würthwein
California Institute of Technology, Pasadena, California 91125

D. M. Asner, D. W. Bliss, W. S. Brower, G. Masek, H. P. Paar, S. Prell, M. Sivertz, and V. Sharma
University of California, San Diego, La Jolla, California 92093

J. Gronberg, T. S. Hill, R. Kutschke, D. J. Lange, S. Menary, R. J. Morrison, H. N. Nelson, T. K. Nelson, C. Qiao, J. D. Richman, D. Roberts, A. Ryd, and M. S. Witherell
University of California, Santa Barbara, California 93106

R. Balest, B. H. Behrens, K. Cho, W. T. Ford, H. Park, P. Rankin, J. Roy, and J. G. Smith
University of Colorado, Boulder, Colorado 80309-0390

0556-2821/98/57(3)/1350(9)/$15.00

J. P. Alexander, C. Bebek, B. E. Berger, K. Berkelman, K. Bloom, D. G. Cassel, H. A. Cho, D. M. Coffman, D. S. Crowcroft, M. Dickson, P. S. Drell, K. M. Ecklund, R. Ehrlich, R. Elia, A. D. Foland, P. Gaidarev, R. S. Galik, B. Gittelman, S. W. Gray, D. L. Hartill, B. K. Heltsley, P. I. Hopman, J. Kandaswamy, P. C. Kim, D. L. Kreinick, T. Lee, Y. Liu, G. S. Ludwig, J. Masui, J. Mevissen, N. B. Mistry, C. R. Ng, E. Nordberg, M. Ogg,[‡] J. R. Patterson, D. Peterson, D. Riley, A. Soffer, B. Valant-Spaight, and C. Ward
Cornell University, Ithaca, New York 14853

M. Athanas, P. Avery, C. D. Jones, M. Lohner, C. Prescott, J. Yelton, and J. Zheng
University of Florida, Gainesville, Florida 32611

G. Brandenburg, R. A. Briere, Y. S. Gao, D. Y.-J. Kim, R. Wilson, and H. Yamamoto
Harvard University, Cambridge, Massachusetts 02138

T. E. Browder, F. Li, Y. Li, and J. L. Rodriguez
University of Hawaii at Manoa, Honolulu, Hawaii 96822

T. Bergfeld, B. I. Eisenstein, J. Ernst, G. E. Gladding, G. D. Gollin, R. M. Hans, E. Johnson, I. Karliner, M. A. Marsh, M. Palmer, M. Selen, and J. J. Thaler
University of Illinois, Champaign-Urbana, Illinois 61801

K. W. Edwards
Carleton University, Ottawa, Ontario, Canada K1S 5B6
and the Institute of Particle Physics, Canada

A. Bellerive, R. Janicek, D. B. MacFarlane, K. W. McLean, and P. M. Patel
McGill University, Montréal, Québec, Canada H3A 2T8
and the Institute of Particle Physics, Canada

A. J. Sadoff
Ithaca College, Ithaca, New York 14850

(CLEO Collaboration)
(Received 7 July 1997; published 13 January 1998)

Using the CLEO detector at the Cornell Electron Storage Ring, we have made a measurement of $R \equiv \sigma(e^+e^- \to \text{hadrons})/\sigma(e^+e^- \to \mu^+\mu^-) = 3.56 \pm 0.01 \pm 0.07$ at $\sqrt{s} = 10.52$ GeV. This implies a value for the strong coupling constant of $\alpha_s(10.52\ \text{GeV}) = 0.20 \pm 0.01 \pm 0.06$, or $\alpha_s(M_Z) = 0.13 \pm 0.005 \pm 0.03$. [S0556-2821(98)05703-8]

PACS number(s): 12.38.Aw, 12.38.Qk, 13.60.Hb, 13.85.Lg

I. INTRODUCTION

The measurement of the hadronic production cross section in e^+e^- annihilation is perhaps the most fundamental experimentally accessible quantity in quantum chromodynamics (QCD) due to its insensitivity to the fragmentation process. The measured hadronic cross section is generally expressed in terms of its ratio R to the point cross section for $\mu^+\mu^-$ production. In QCD, R is directly proportional to the number of colors, depends on quark charges, and varies with energy, both discretely as quark mass thresholds are crossed and gradually as the strong coupling constant α_s ''runs.'' R measurements have been valuable in verifying quark thresholds, charges, color counting, and the existence of the gluon.

The theoretical prediction for R, expressed as an expansion in powers of α_s/π, is

$$R = R_{(0)}[1 + \alpha_s/\pi + C_2(\alpha_s/\pi)^2 + C_3(\alpha_s/\pi)^3]. \quad (1)$$

$R_{(0)}$ is the lowest-order prediction for this ratio, given by $R_{(0)} = N_c \Sigma_i q_i^2$, where N_c is the number of quark colors; the sum runs over the kinematically allowed quark flavors. Just below the $\Upsilon(4S)$ resonance, where $b\bar{b}$ production is kinematically forbidden, the lowest-order prediction is therefore obtained by summing over $udcs$ quarks, yielding $R_{(0)} = 10/3$. The α_s corrections contribute an additional $\sim 15\%$ to this value. A calculation appropriate at CERN e^+e^- collider LEP energies obtained $C_2 = 1.411$ and $C_3 = -12.68$ [1] for five active flavors, in the limit of massless quarks. A recent calculation, applicable to the Υ mass region (four active flavors), has included corrections due to the effects of quark masses and QED radiation to obtain $C_2 = 1.5245$ and $C_3 = -11.52$ at $\sqrt{s} = 10$ GeV [2]. The effect of including these additional corrections is a difference of approximately

*Permanent address: BINP, RU-630090 Novosibirsk, Russia.

†Permanent address: Lawrence Livermore National Laboratory, Livermore, CA 94551.

‡Permanent address: University of Texas, Austin, TX 78712.

0.3% in the prediction for R at this energy. In this article we present a measurement of R using the CLEO detector operating at the Cornell Electron Storage Ring (CESR) at a center-of-mass energy $\sqrt{s}=10.52$ GeV.

II. APPARATUS AND EVENT SELECTION

The CLEO II detector is a general purpose solenoidal magnet spectrometer and calorimeter [3]. The detector was designed to trigger efficiently on two-photon, tau-pair, and hadronic events. As a result, although hadronic event reconstruction efficiencies are high, lower-multiplicity nonhadronic backgrounds require careful consideration in this analysis. Good background rejection is afforded by the high-precision electromagnetic calorimetry and excellent charged-particle-tracking capabilities. Charged particle momenta are measured with three nested coaxial drift chambers with 6, 10, and 51 layers, respectively. These chambers fill the volume from $r=3$ cm to $r=100$ cm, where r is the radial coordinate relative to the beam (z) axis, and have good efficiency for charged particle tracking for polar angles $|\cos\theta|<0.94$, with θ measured relative to the positron beam direction ($+\hat{z}$). This system achieves a momentum resolution of $(\delta p/p)^2=(0.0015p)^2+(0.005)^2$, where p is the momentum in GeV/c. Pulse height measurements in the main drift chamber provide a specific ionization resolution of 6.5% for Bhabha events, giving good K/π separation for tracks with momenta up to 700 MeV/c and approximately two standard deviation resolution in the relativistic rise region. Outside the central tracking chambers are plastic scintillation counters that are used as fast elements in the trigger system and also provide particle identification information from time-of-flight measurements. Beyond the time-of-flight system is the electromagnetic calorimeter, consisting of 7800 thallium-doped cesium iodide crystals. The central ''barrel'' region of the calorimeter covers about 75% of the solid angle and has an energy resolution of about 4% at 100 MeV and 1.2% at 5 GeV. Two end cap regions of the crystal calorimeter extend solid angle coverage to about 98% of 4π, although with somewhat worse energy resolution than the barrel region. The tracking system, time-of-flight counters, and calorimeter are all contained within a 1.5 T superconducting coil.

To suppress $\tau\tau$, $\gamma\gamma$, low-multiplicity QED, and other backgrounds while maintaining relatively high $q\bar{q}$ event reconstruction efficiency, we impose several requirements to enrich our hadronic event sample. To suppress events originating as collisions of $e^{\pm}$ beam particles with gas or the vacuum chamber walls, we require that the reconstructed event vertex (defined as $z_{\rm vrtx}$) be within 6 cm in z ($\hat{z}$ defined above as the e^+ beam direction) and 2 cm in cylindrical radius of the nominal interaction point. Figure 1 displays the distribution in the z coordinate. Single-beam backgrounds are expected to be flat in this distribution; hadronic events peak at $z=0$ with a resolution of approximately 2 cm. Other event selection criteria are imposed on various kinematic quantities. To illustrate the effect of these selection requirements, we show below distributions from data; Monte Carlo comparisons are also shown. Simulated hadronic events are produced using the JETSET 7.3 $q\bar{q}$ event generator [4] run through a full GEANT-based [5] CLEO-II detector simulation.

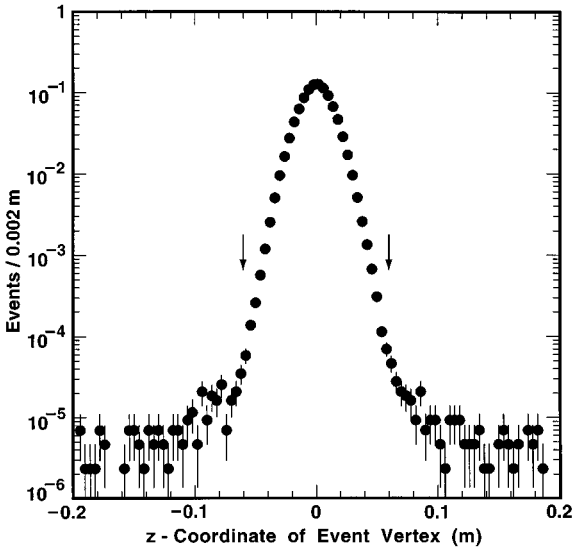

FIG. 1. Distribution of the z coordinate of the event vertex for candidate hadronic events. Arrows indicate the location of cuts.

Tau-pair events use the KORALB [6] event generator in conjunction with the same detector simulation.[1] We also use this Monte Carlo event sample to determine the efficiency for $q\bar{q}$ and $\tau\tau$ events to pass the following hadronic event selection requirements: (1) At least five detected, good quality, charged tracks ($N_{\rm chrg}\geq 5$, as shown in Fig. 2); (2) the total visible energy $E_{\rm vis}$ ($=E_{\rm chrg}+E_{\rm neutral}$) should be greater than the single beam energy, $E_{\rm vis}>E_{\rm beam}$ (Fig. 3); (3) The z component of the missing momentum must satisfy $|P_z^{\rm miss}|/E_{\rm vis}<0.3$ (Fig. 4).

In addition to these primary requirements, additional criteria are imposed to remove backgrounds remaining at the $\sim$1% level, as well as to suppress events with hard initial state radiation, for which theoretical uncertainties are large. These are the following:

(a) No more than two identified electrons are in the event.

(b) The ratio R_2 of the second to the zeroth Fox-Wolfram moments [7] for the event should satisfy $R_2<0.9$ (Fig. 5). As can be seen from the figure, the separation between Monte Carlo $q\bar{q}$ and $\tau\tau$ events is quite good, and the inclusion of the $\tau\tau$ component significantly improves the fit.[2]

(c) The ratio of calorimeter energy contained in showers that match to charged particles divided by the beam energy ($E_{\rm calorimeter}^{\rm charged\ tracks}/E_{\rm beam}$) must be less than 0.9 (Fig. 6).

(d) We impose a requirement on the highest-energy photon in an event—the most energetic photon candidate de-

[1]In the comparison plots, both the data and the ''Monte Carlo sum'' have been normalized to unit area in the ''good'' acceptance region. All remaining hadronic event selection requirements save for the one being displayed have been imposed.

[2]In fact, we can determine the $q\bar{q}$ and $\tau\tau$ fractions by fitting the R_2 distribution to the sum of the expected $q\bar{q}$ and $\tau\tau$ R_2 shapes, with only the relative normalizations floating. Such a fit gives a value of the $\tau\tau$ fraction which is consistent with that calculated using the expected relative tau pair and $q\bar{q}$ production cross sections and efficiencies.

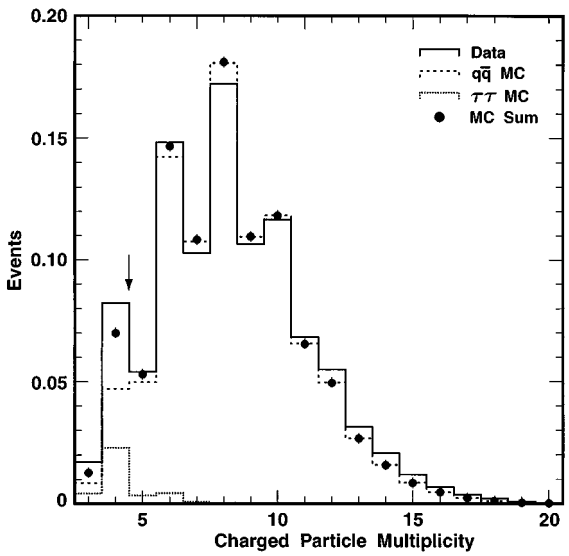

FIG. 2. Normalized charged multiplicity distribution for data (solid line), $q\bar{q}$ Monte Carlo simulations (dashed line), and $\tau\tau$ Monte Carlo simulations (dotted line). Sum of $q\bar{q}$ plus $\tau\tau$ Monte Carlo simulations is shown as solid circles.

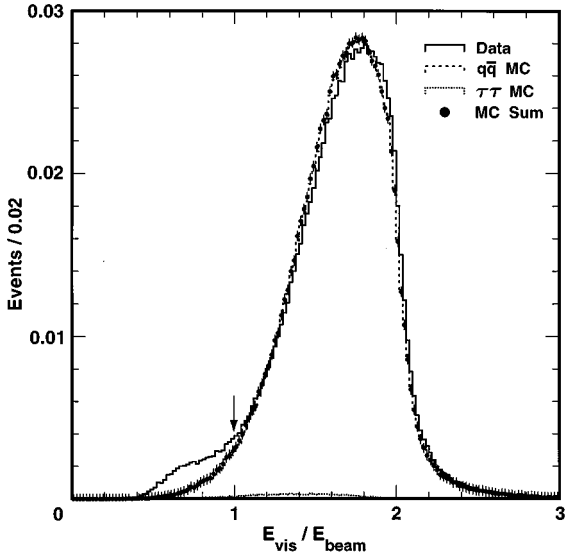

FIG. 3. Normalized visible energy distribution for data (solid line), $q\bar{q}$ Monte Carlo simulations (dashed line), and $\tau\tau$ Monte Carlo simulations (dotted line). Sum of $q\bar{q}$ plus $\tau\tau$ Monte Carlo simulations is shown as solid circles. The excess in the region $E_{\rm vis}/E_{\rm beam}<1$ is attributed primarily to two-photon collisions.

tected in the event must have a measured energy less than 0.75 of the beam energy ($x_\gamma \equiv E_\gamma^{\rm max}/E_{\rm beam}<0.75$), as shown in Fig. 7. This requirement also reduces the uncertainty from radiative corrections, as discussed later.

We note that, according to the Monte Carlo simulation, the trigger inefficiency with the default event selection criteria is less than 0.1%. This has been checked with the data by counting the fraction of events classified as ''hadronic'' which trigger only a minimum bias, prescaled trigger line.

III. BACKGROUNDS

After imposition of the above hadronic event selection criteria, we are left with a sample of 4.00×10^6 candidate hadronic events. Agreement between data and Monte Carlo simulations is, at this point, rather good, as illustrated in Figs. 8, 9, and 10, which show the distributions in the z component of the missing momentum, the z component of the event thrust axis, and the scaled event transverse momentum, respectively. Nevertheless, small backgrounds still remain. These are enumerated as follows.

(1) Backgrounds from $e^+e^-\to\tau^+\tau^-(\gamma)$ events are subtracted statistically using a large Monte Carlo sample of KORALB tau-pair events. These events comprise $(1.3\pm0.1)\%$ (statistical error only) of the sample passing the above event selection criteria.

(2) Contributions from the narrow Υ resonances [the (1S), (2S), and (3S) states] are determined from a combination of data and theoretical calculation. Backgrounds from radiative production of the $\Upsilon(3S)$ and $\Upsilon(2S)$ resonances are assessed using $e^+e^-\to\gamma\Upsilon(3S/2S)$, $\Upsilon(3S/2S)\to\pi^+\pi^-\Upsilon(1S)$, $\Upsilon(1S)\to l^+l^-$ events in data. These events are distinctive by their characteristic topology of two low-momentum pions accompanied by two very-high-momentum, back-to-back leptons; the photon generally escapes undetected along the beam axis. As shown in Fig. 11, we observe these events as distinct peaks in the mass distribution recoiling against two low-momentum pions in events also containing two high-energy muons. [The recoil mass is calculated from $M_{\rm recoil}=\sqrt{(2E_{\rm beam}-E_{\pi_1}-E_{\pi_2})^2-(\vec{p}_{\pi_1}+\vec{p}_{\pi_2})^2}$, and therefore neglects the four-momentum of the initial state radiation photon. This calculated recoil mass is thus the sum of the $\Upsilon(1S)$ and the undetected photon four-vectors.] Knowing the branching fractions [8] for $\Upsilon(2S)\to\pi\pi\Upsilon(1S)$ $(18.5\pm0.8\%)$ and $\Upsilon(3S)\to\pi\pi\Upsilon(1S)$ $(4.5\pm0.2\%)$, the leptonic branching fraction for the $\Upsilon(1S)$ $(2.5\pm0.1)\%$, and the reconstruction

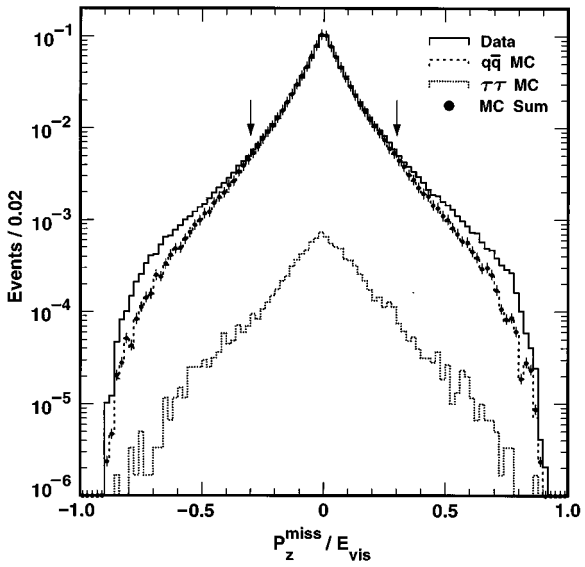

FIG. 4. Ratio of $P_z^{\rm miss}/E_{\rm visible}$ for data vs Monte Carlo simulations. Two-photon collisions and beam-gas interactions tend to populate the regions away from zero and towards ±1 in this plot.

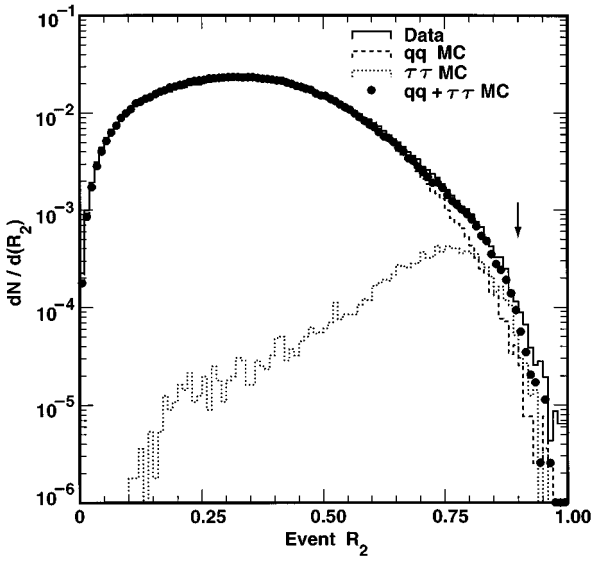

FIG. 5. Ratio of Fox-Wolfram moments $R2=H_2/H_0$ for data vs Monte Carlo calculation.

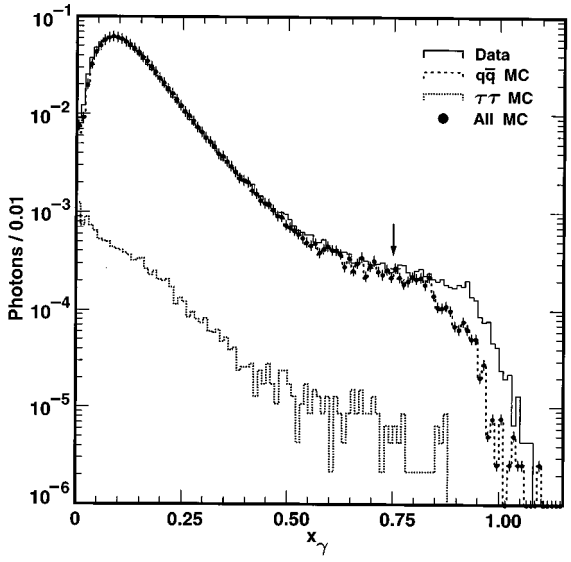

FIG. 7. Comparison of data vs Monte Carlo spectrum of most energetic photon observed in event.

efficiency for such events (~ 0.7), we can determine the contribution to the observed hadronic cross section from the $\Upsilon(2S)$ and $\Upsilon(3S)$ resonances directly, by simply measuring the event yields in the peaks shown in Fig. 11, and correcting by branching fractions and efficiency.

We have estimated the contribution from $\gamma\Upsilon(1S)$ events in two ways. First, we assume that the initial state photon spectrum varies as $dN/dE_\gamma \sim 1/E_\gamma$, and that the production of a given Υ resonance is proportional to its dielectron width Γ_{ee}. This gives a fairly simple prediction for the cross sections expected for the three narrow Υ resonances, since $E_\gamma \sim (10.52 - M_\Upsilon)$ GeV. We would expect that the production cross section for $\Upsilon\gamma$ in e^+e^- annihilation therefore varies as $\Gamma(e^+e^- \to \Upsilon\gamma) \propto \Gamma_{ee}^{\Upsilon}/E_\gamma$. This allows us to infer an expected production cross section for $\gamma\Upsilon(1S)$ based on our measurements for $\gamma\Upsilon(2S)$ and $\gamma\Upsilon(3S)$ production. Theory [2] also prescribes what the magnitude of these corrections should be. We compare our extrapolated cross section for $e^+e^- \to \gamma\Upsilon(1S)$ through the simpleminded procedure outlined above with the theoretical calculation for this correction in order to estimate the total magnitude of this correction, and its associated error. We determine that the sum of $\gamma\Upsilon(1S)$, $\gamma\Upsilon(2S)$, and $\gamma\Upsilon(3S)$ events comprise $(1.8 \pm 0.6)\%$ of the observed hadronic cross section, where the error includes the uncertainties in the Υ decay branching fractions and detection efficiencies as well as the deviations between the estimates from theoretical calculation and data.

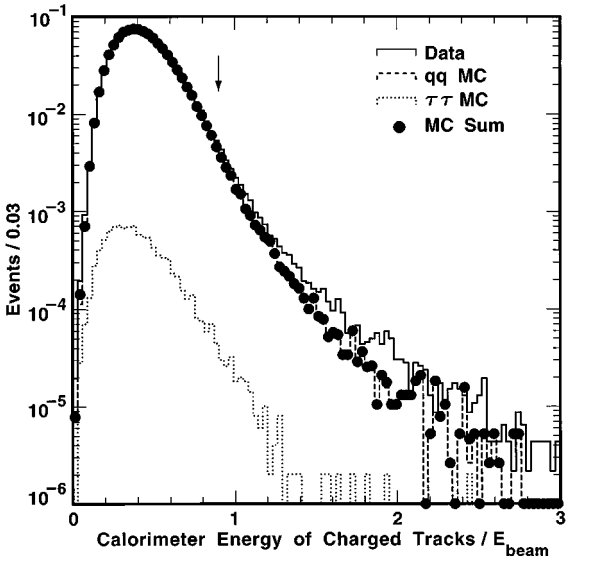

FIG. 6. Comparison of data vs Monte Carlo distribution of calorimeter energy deposited by charged tracks relative to the beam energy in an event.

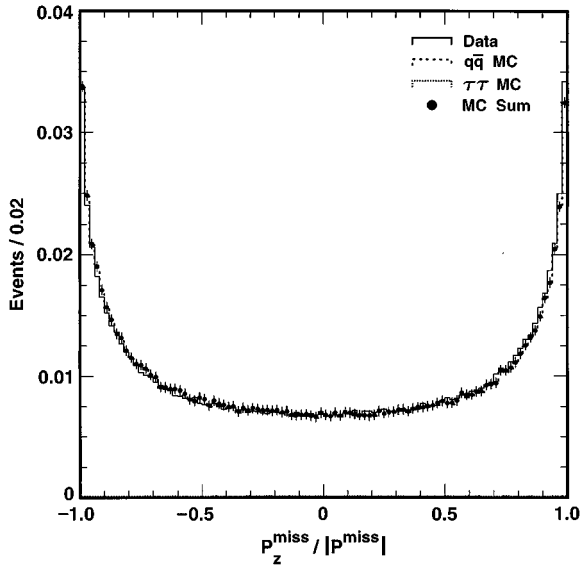

FIG. 8. Distribution of the z component (i.e., direction cosine) of the missing momentum $P_z^{\rm miss}/|P^{\rm miss}|$ for data vs Monte Carlo simulations, after application of all hadronic event selection requirements (this variable is not cut on).

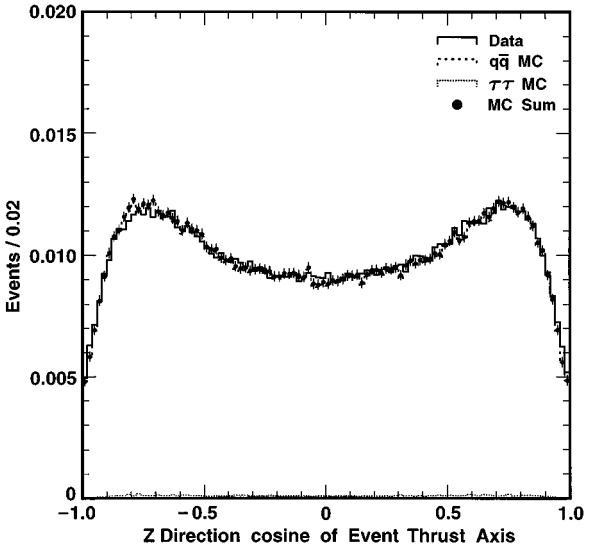

FIG. 9. z component of the thrust axis for data vs Monte Carlo calculation, after application of all hadronic event selection requirements (this variable is not cut on).

(3) Two-photon collisions, which produce hadrons in the final state via $e^+e^- \to e^+e^- \gamma\gamma \to e^+e^-$ +hadrons, are determined by running final-state specific $\gamma\gamma$ collision Monte Carlo events, and also by determining the magnitude of possible excesses in the E_{visible} vs $P_{\text{transverse}}$ plane for data over $q\bar{q}$ Monte Carlo calculation. Figure 12 shows the visible energy vs transverse momentum distribution for events which are $e^+e^- \to \gamma\gamma e^+e^-$ depleted (left, obtained by requiring our default hadronic event selection requirements, save for the requirement that the total visible energy exceed the beam energy) and $e^+e^- \to \gamma\gamma e^+e^-$ enriched (right, obtained by requiring $|P_z^{\text{miss}}|/E_{\text{vis}} > 0.3$ and $N_{\text{chrg}} = 3$ or 4). We notice the presence of a prominent peak in the $\gamma\gamma$-enriched

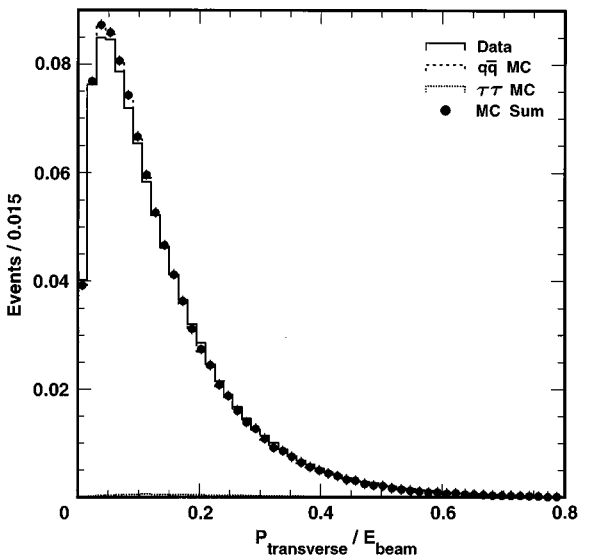

FIG. 10. Ratio of transverse momentum relative to beam energy, after application of all hadronic event selection requirements (this variable is not cut on).

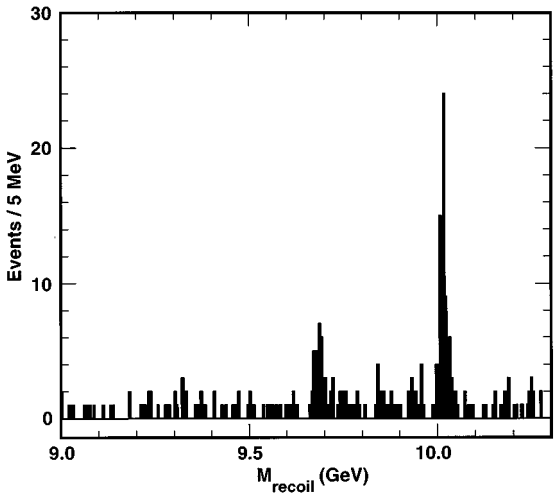

FIG. 11. Mass recoiling against two charged particles, assumed to be pions, in events consistent with the kinematics for $e^+e^- \to \gamma\Upsilon(3S/2S)$, $\Upsilon(3S/2S) \to \Upsilon(1S)\pi^+\pi^-$, $\Upsilon(1S) \to l^+l^-$. Two peaks are evident; the leftmost peak corresponds to $\Upsilon(3S) \to \pi^+\pi^-\Upsilon(1S)$ transitions, the rightmost peak corresponds to $\Upsilon(2S) \to \pi^+\pi^-\Upsilon(1S)$ transitions. The calculated recoil mass differs from the true $\Upsilon(1S)$ mass due to our neglecting the (undetected) radiated photon in the recoil mass calculation.

sample at low values of the transverse momentum and small visible energy. We can use the shape of this peak to estimate the possible residual contamination from two-photon collisions remaining in the $\gamma\gamma$-poor distribution after imposition of all our hadronic event selection requirements. Two-photon collisions are thus determined to comprise $(0.8 \pm 0.4)\%$ of our total hadronic event sample.

(4) Beam-wall, beam-gas, and cosmic ray events are expected to have a flat event vertex distribution in the interval

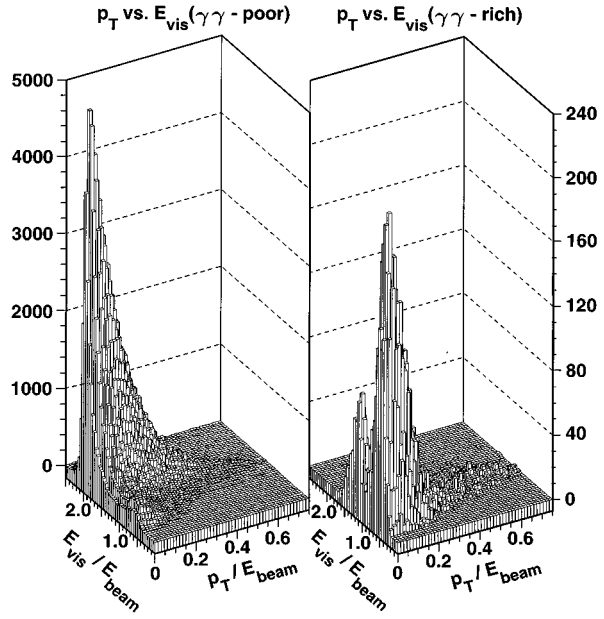

FIG. 12. Distribution of transverse momentum vs visible energy for event samples depleted (left) and enriched (right) in $e^+e^- \to \gamma\gamma e^+e^-$, $\gamma\gamma \to$hadrons events.

$|z_{\rm vrtx}|<10$ cm. Figure 1 shows the distribution in the z coordinate of the event vertex for events passing the remainder of our hadronic event selection requirements. The contribution of such events is estimated by extrapolating the yield of events having a vertex in the interval 6 cm$<|z_{\rm vrtx}|<10$ cm into the ''good'' acceptance region ($|z_{\rm vrtx}|<6$ cm). These backgrounds are determined to comprise $\sim(0.2\pm0.1)\%$ of our hadronic sample.

(5) Remaining QED backgrounds producing more than two electrons or muons in the final state are assessed using a high-statistics sample of Monte Carlo events (to 3$^{\rm rd}$ order in $\alpha_{\rm QED}$), and found to comprise $\leqslant 0.1\%$ of the sample passing the above hadronic event selection requirements.

Summing these estimates results in a net background fraction $f=(4.1\pm0.7)\%$. We note that, as this error is assessed partly by examining the difference between Monte Carlo hadronic event simulations and our data, this error also includes Monte Carlo modeling errors.

IV. EFFICIENCIES AND RADIATIVE CORRECTIONS

The computation of R is peformed with

$$R=\frac{N_{\rm had}(1-f)}{\mathcal{L}\epsilon_{\rm had}(1+\delta)\sigma^0_{\mu\mu}}, \tag{2}$$

where $N_{\rm had}$ is the number of events classified as hadronic, f is the fraction of selected events attributable to all background processes, $\epsilon_{\rm had}$ is the efficiency for triggering and selection of events, δ is the fractional increase in hadronic cross section due to electromagnetic radiative corrections, $\sigma^0_{\mu\mu}$ is the point cross section for muon pair production [86.86 nb/$E^2_{\rm c.m.}$ (GeV^2)], and $\mathcal{L}$ is the measured integrated luminosity. The luminosity is determined from wide angle e^+e^-, $\gamma\gamma$, and $\mu^+\mu^-$ final states and is known to $\pm1\%$ [9]. For the data analyzed here, the integrated luminosity $\mathcal{L}$ is equal to (1.521 ± 0.015) fb^{-1}.

To calculate R, we must therefore evaluate Eq. (2). If the initial-state radiation corrections were known precisely, we would be able to calculate the denominator term $\epsilon(1+\delta)$ with very good precision. However, since the uncertainties become very large as the center-of-mass energy approaches the $c\bar{c}$ threshold ($\sqrt{s}\sim4$ GeV), the preferred procedure is to choose some explicit cutoff in the initial-state radiation (ISR) photon energy that makes us as insensitive as possible to the corrections in this high-ISR-photon-energy–low-hadronic-recoil-mass region. We therefore purposely design our selection criteria so that our acceptance for events with highly energetic ISR photons approaches zero. By choosing cuts that drive ϵ to zero beyond some kinematic point, we ensure that the product $\epsilon\times(1+\delta)$ is insensitive to whatever value of δ may be prescribed by theory beyond our cut. Thus, although there is a large uncertainty in the magnitude of the initial-state radiation correction for large values of radiated photon momentum, we have minimized our sensitivity to this theoretical uncertainty. Figure 13 displays our acceptance for an $e^+e^-\to\gamma q\bar{q}$ event to pass our hadronic event criteria as a function of the scaled photon energy $x_\gamma\equiv E_\gamma/E_{\rm beam}$. Based on the agreement between data and Monte Carlo simulations shown in Fig. 7, we have applied a cut on the maximum

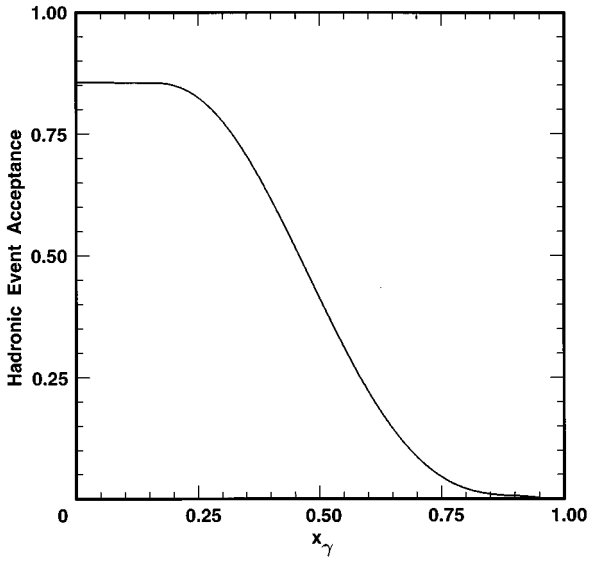

FIG. 13. Acceptance for $e^+e^-\to\gamma q\bar{q}$ events as a function of the scaled photon momentum $x_\gamma\equiv E_\gamma/E_{\rm beam}$.

energy allowed for a single shower in an event: $x_\gamma<0.75$. We note that for $x_\gamma>0.75$ (corresponding to a $q\bar{q}$ recoil mass of $M_{\rm recoil}<5.25$ GeV/c^2), our integrated event-finding acceptance $\epsilon_{\rm had}<1\%$. For $x_\gamma>0.75$, we have therefore minimized our sensitivity to modeling uncertainties in this kinematic regime—increasing (theoretically) the initial-state radiation contribution to this high-x_γ region results in a compensating loss of overall acceptance such that the product of $\epsilon(1+\delta)$ remains relatively constant. Our event selection criteria thus corresponds to a value of $\epsilon(1+\delta)(x_\gamma^{\rm max}=0.75)=0.90\pm0.01$, where the error reflects the systematic uncertainty in the radiative corrections.

After subtracting all backgrounds, dividing by the total luminosity, and normalizing to the mu-pair point cross section, we obtain a value of $R=3.56\pm0.01$ (statistical error only, including statistical errors in data, Monte Carlo statistics, and the statistics of the sample used to calculate our luminosity).

V. SYSTEMATIC ERRORS AND CONSISTENCY CHECKS

We have checked our results in several ways. Backgrounds can be suppressed significantly by tightening the minimum charged track multiplicity to $N_{\rm chrg}\geqslant7$, albeit at a loss of $\sim20\%$ in the overall event-reconstruction efficiency. Imposition of such a cut leads to only a -0.4% change in the calculated value of R. Continuum data have been collected over 17 distinct periods from 1990 to 1996, covering many different trigger configurations and running conditions. We find a 0.3% rms variation between the various data sets used (the statistical error on R within each data set is of order 0.1%). We can check contributions due to the narrow Υ resonances by calculating R using a small amount (5 pb^{-1}) of continuum data taken just below the $\Upsilon(2S)$ resonance, at $E_{\rm beam}=4.995$ GeV. At this center-of-mass energy, we are insensitive to corrections from $e^+e^-\to\gamma\Upsilon(3S)$ and $e^+e^-\to\gamma\Upsilon(2S)$. We find that the value of R calculated using the $\Upsilon(2S)$ continuum agrees with that calculated using the $\Upsilon(4S)$

TABLE I. Systematic errors in R analysis.

Source	Error
$\epsilon\times(1+\delta)$	1%
$\mathcal{L}$	1%
Background uncertainty/hadronic event modeling uncertainty	0.7%
Data-set–to–data-set variation	0.3%
Total	1.8%

continuum to within one statistical error ($1\sigma_{\rm stat}$). Systematic errors are summarized in Table I.

VI. EXTRACTION OF α_s

Using the expansion for R in powers of α_s/π given previously, with coefficients appropriate for this center-of-mass energy [2], we can evaluate the strong coupling constant, using the prescription outlined by the Particle Data Group [8]. Using that expression, our value for R translates to $\alpha_s(10.52\ \text{GeV})=0.20\pm0.01\pm0.06$.

To compare this α_s value with measurements at the Z^0, we need to extrapolate our result to $\sqrt{s}=90$ GeV. The strong coupling constant $\alpha_{\rm s}$ can be written as a function of the basic QCD parameter $\Lambda_{\overline{\rm MS}}$, defined in the modified minimal subtraction scheme [8] as

$$\alpha_{\rm s}(\mu)=\frac{4\pi}{b_0 x}\left\{1-\frac{2b_1}{b_0^2}\frac{\ln(x)}{x}+\frac{4b_1^2}{b_0^4x^2}\left(\left[\ln(x)-\frac{1}{2}\right]^2+\frac{b_2b_0}{8b_1^2}-\frac{5}{4}\right)\right\}, \tag{3}$$

where $b_0=(11-2n_f/3)$, μ is the energy scale, in GeV, at which α_s is being evaluated, $b_1=(51-19n_f)/3$, $b_2=2857-5033n_f/9+325n_f^2/27$, $x=\ln(\mu^2/\Lambda^2_{\overline{\rm MS}})$, and n_f is the number of light quark flavors which participate in the process. To determine the value of $\alpha_s(90\ \text{GeV})$ implied by our measurement, we must evolve α_s across the discontinuity in $\Lambda_{\overline{\rm MS}}$ when the five-flavor threshold is crossed from the four-flavor regime. We do so using the next-to-next-to-leading order (NNLO) prescription, as described in [8]: (a) We substitute $\alpha_s(10.52)$ into Eq. (3) to determine a value for $\Lambda_{\overline{\rm MS}}$ in the four-flavor continuum [obtaining $\Lambda_{\overline{\rm MS}}(udcs)=498$ MeV]. (b) With that value of $\Lambda_{\overline{\rm MS}}$, we can now again use Eq. (3) to determine the value of α_s at the five-flavor threshold when the b-quark pole mass (we use $m_{b,\rm pole}=4.7$ GeV) is crossed, and then use that value of α_s, as well as $n_f=5$ in Eq. (3) to determine $\Lambda_{\overline{\rm MS}}$ appropriate for the five-flavor continuum. (c) Assuming that this value of $\Lambda_{\overline{\rm MS}}$ is constant in the entire five-flavor energy region, we can now evolve α_s up to the Z pole, to obtain $\alpha_s(M_Z)=0.13\pm0.005\pm0.03$, in good agreement with the world average $\alpha_s(M_Z)=0.118\pm0.003$ [8].

TABLE II. Summary of inclusive cross section measurements.

Experiment	$\sqrt{s}$ (GeV)	R
PLUTO [10]	9.4	$3.67\pm0.23\pm0.29$
DASPII [11]	9.4	$3.37\pm0.16\pm0.28$
DESY-Heidelberg [12]	9.4	$3.80\pm0.27\pm0.42$
LENA [13]	9.1-9.4	$3.34\pm0.09\pm0.18$
LENA [13]	7.4-9.4	$3.37\pm0.06\pm0.23$
CUSB [14]	10.5	$3.54\pm0.05\pm0.40$
CLEO 83 [15]	10.5	$3.77\pm0.06\pm0.24$
Crystal Ball [16]	9.4	$3.48\pm0.04\pm0.16$
ARGUS [17]	9.36	$3.46\pm0.03\pm0.13$
MD-1 [18]	7.25-10.34	$3.58\pm0.02\pm0.14$
Previous experiments, weighted average	≈9.5	3.58 ± 0.07
CLEO 97 (this work)	10.5	$3.56\pm0.01\pm0.07$

VII. SUMMARY

Near $\sqrt{s}=10$ GeV, R has been measured by many experiments, as shown in Table II. The measurement of R described here is the most precise below the Z^0. Our R value is in good agreement with the previous world average, including a recent determination by the MD-1 Collaboration [18]. Our implied value of α_s is in agreement with higher-energy determinations of this quantity. Theoretical uncertainties in QED radiative corrections (in the acceptance $[\epsilon\times(1+\delta)]$ and luminosity [9]) contribute about the same amount to the systematic error as do backgrounds and efficiencies. Substantial improvements in this measurement will require progress on radiative corrections as well as on experimental techniques.

ACKNOWLEDGMENTS

We gratefully acknowledge the effort of the CESR staff in providing us with excellent luminosity and running conditions. J.P.A., J.R.P., and I.P.J.S. thank the NYI program of the NSF, M.S. thanks the PFF program of the NSF, G.E. thanks the Heisenberg Foundation, K.K.G., M.S., H.N.N., T.S., and H.Y. thank the OJI program of DOE, J.R.P., K.H., M.S., and V.S. thank the A.P. Sloan Foundation, R.W. thanks the Alexander von Humboldt Stiftung, and M.S. thanks Research Corporation for support. This work was supported by the National Science Foundation, the U.S. Department of Energy, and the Natural Sciences and Engineering Research Council of Canada.

[1] S. G. Gorishny, A. L. Kataev, and S. A. Larin, Phys. Lett. B **259**, 144 (1991): L. R. Surguladze and M. A. Samuel, Phys. Rev. Lett. **66**, 560 (1991); K. G. Chetyrkin, Phys. Lett. B **391**, 402 (1997).

[2] K. G. Chetyrkin, J. H. Kühn, and T. Teubner, Phys. Rev. D **56**, 3011 (1997); K. G. Chetyrkin and J. H. Kühn, Phys. Lett. B **342**, 356 (1995); **308**, 127 (1993).

[3] CLEO Collaboration, Y. Kubota *et al.*, Nucl. Instrum. Meth-

ods Phys. Res. A **320**, 66 (1992).
[4] S. J. Sjostrand, LUND 7.3, CERN Report No. CERN-TH-6488-92, 1992.
[5] R. Brun *et al.*, GEANT, version 3.14, CERN Report No. CERN CC/EE/84-1, 1987.
[6] We use KORALB, version 2.2, and TAUOLA, version 2.4. References for earlier versions are S. Jadach and Z. Was, Comput. Phys. Commun. **36**, 191 (1985); **64**, 267 (1991); S. Jadach, J. H. Kühn, and Z. Was, *ibid.* **64**, 275 (1991); **70**, 69 (1992); **76**, 361 (1993).
[7] G. C. Fox and S. Wolfram, Phys. Rev. Lett. **41**, 1581 (1978); Phys. Lett. **82B**, 134 (1979).
[8] Particle Data Group, R. M. Barnett *et al.*, Phys. Rev. D **54**, 1 (1996).
[9] CLEO Collaboration, G. Crawford *et al.*, Nucl. Instrum. Methods Phys. Res. A **345**, 429 (1994).
[10] The PLUTO Collaboration, L. Criegee *et al.*, Phys. Rep. **83**, 151 (1982).
[11] The DASP-II Collaboration, H. Albrecht *et al.*, Phys. Lett. **116B**, 383 (1982).
[12] P. Bock *et al.*, Z. Phys. C **6**, 125 (1980).
[13] LENA Collaboration, B. Niczporuck *et al.*, Z. Phys. C **15**, 299 (1982).
[14] The CUSB Collaboration, E. Rice *et al.*, Phys. Rev. Lett. **48**, 906 (1982).
[15] The CLEO Collaboration, R. Giles *et al.*, Phys. Rev. D **29**, 1285 (1984).
[16] The Crystal Ball Collaboration, Z. Jakubowski *et al.*, Z. Phys. C **49**, 49 (1988).
[17] The ARGUS Collaboration, H. Albrecht *et al.*, Z. Phys. C **53**, 13 (1991).
[18] The MD-1 Collaboration, A. E. Blinov *et al.*, Z. Phys. C **70**, 31 (1996).